FINAL REPORT

Groundwater Flooding on Highways in the Nebraska Sandhills: Applying Remote Sensing, Precipitation and Groundwater Modeling to Determine Depth, Cause and Frequency

Aaron Mittelstet

Biological Systems Engineering Department

University of Nebraska-Lincoln

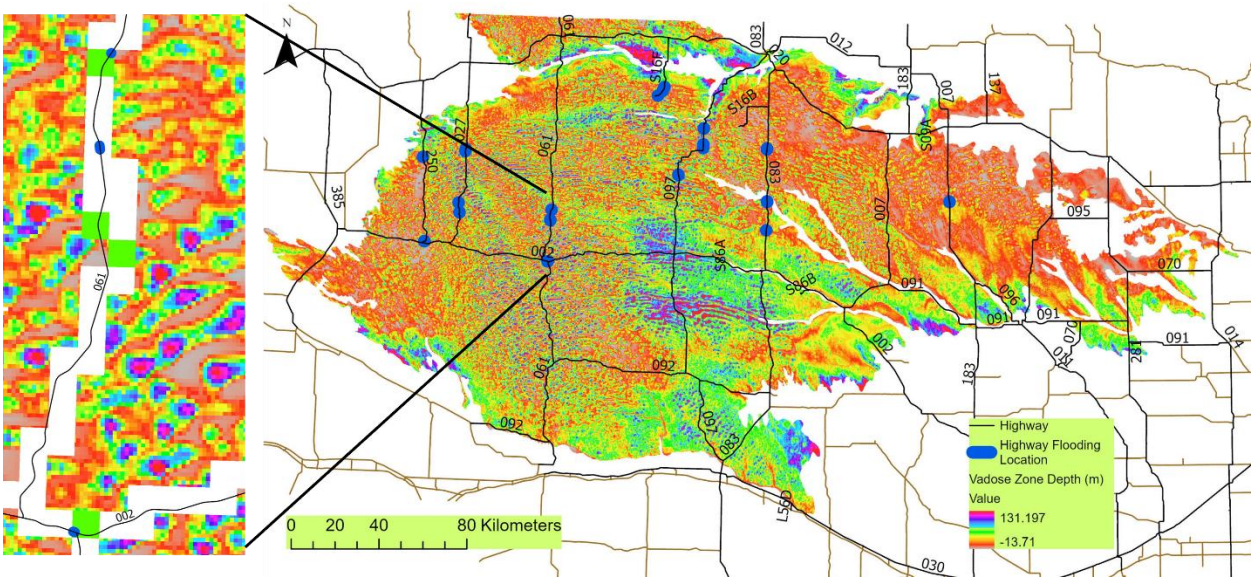

Sponsored By

Nebraska Department of Transportation and U.S. Department of Transportation Federal Highway Administration

June 2025

TECHNICAL REPORT DOCUMENTATION PAGE

1. Report No. SPR-FY22(005)	2. Government Accession No.	3. Recipient's Catalog No.
4. Title and Subtitle Groundwater Flooding on Highways in the Nebraska Sandhills: Applying Remote Sensing, Precipitation and Groundwater Modeling to Determine Depth, Cause and Frequency		**5. Report Date** June 31, 2025 **6. Performing Organization Code**
7. Author(s) Aaron Mittelstet, Principal Investigator		**8. Performing Organization Report No.** If applicable, enter any/all unique numbers assigned to the performing organization.
9. Performing Organization Name and Address University of Nebraska – Lincoln Biological Systems Engineering Department 200 L.W. Chase Hall, E Campus Mall, Lincoln, NE 68583		**10. Work Unit No.** **11. Contract** SPR-FY22(005)
12. Sponsoring Agency Name and Address Nebraska Department of Transportation Research Section 1400 Hwy 2, Lincoln, NE 68502		**13. Type of Report and Period Covered** Final Report 07/2021 – 06/2025 **14. Sponsoring Agency Code**
15. Supplementary Notes		

16. Abstract

Climate change significantly impacts infrastructure sustainability, particularly through shifts in precipitation patterns, intensity, and duration. These precipitation dynamics may increase the occurrence of surface water and groundwater flooding. Groundwater in the Nebraska Sand Hills (NSH), including the thickest portions of the High Plains Aquifer, extends close to the land surface in interdunal areas, making the NSH vulnerable to groundwater flooding. Recent events involving heavy precipitation, snow melt, and rising groundwater levels have caused prolonged highway flooding, disrupting transportation networks. This study estimates groundwater flood inundation depth, duration and frequency in the highways of NSH using remote sensing techniques and groundwater modeling. Results indicate that in 2019, 18 highway sections experienced inundation depths ranging from 0.04 to 0.63 m for up to five months. This flooding was not caused by a single storm event but resulted from cumulative precipitation in 2018 and 2019. Using MODFLOW, we analyzed historical flooding (> 1 m increase in water level over a one- and two-year period) from 1940 to 2009 for ten highways within the NSH and model domain. Flooding frequencies ranged from 0% to 2.7% and from 1.4% to 11% for the two-year periods. These findings provide critical insights for the Nebraska Department of Transportation to prioritize highway improvement efforts in mitigating future flood risks through future construction projects to raise these highways. Observed trends in increasing precipitation, stream discharge and groundwater levels over recent decades, and their role in contributing to major flood events in 2010 and 2019, flooding risks may escalate in the future.

17. Key Words	18. Distribution Statement
Groundwater, Remote Sensing, Floods	No restrictions. This document is available through the National Technical Information Service. 5285 Port Royal Road, Springfield, VA 22161

19. Security Classification (of this report)	20. Security Classification (of this page)	21. No. of Pages	22. Price
Unclassified	Unclassified	40	

Form DOT F 1700.7 (8-72) Reproduction of completed page authorized

DISCLAIMER

The contents of this report reflect the views of the authors, who are responsible for the facts and the accuracy of the information presented herein. The contents do not necessarily reflect the official views or policies neither of the Nebraska Department of Transportations nor the University of Nebraska-Lincoln. This report does not constitute a standard, specification, or regulation. Trade or manufacturers' names, which may appear in this report, are cited only because they are considered essential to the objectives of the report.

The United States (U.S.) government and the State of Nebraska do not endorse products or manufacturers. This material is based upon work supported by the Federal Highway Administration under SPR-FY22(005). Any opinions, findings and conclusions or recommendations expressed in this publication are those of the author(s) and do not necessarily reflect the views of the Federal Highway Administration.

Abstract:

Climate change significantly impacts infrastructure sustainability, particularly through shifts in precipitation patterns, intensity, and duration. These precipitation dynamics may increase the occurrence of surface water and groundwater flooding. Groundwater in the Nebraska Sand Hills (NSH), including the thickest portions of the High Plains Aquifer, extends close to the land surface in interdunal areas, making the NSH vulnerable to groundwater flooding. Recent events involving heavy precipitation, snow melt, and rising groundwater levels have caused prolonged highway flooding, disrupting transportation networks. This study estimates groundwater flood inundation depth, duration and frequency in the highways of NSH using remote sensing techniques and groundwater modeling. Results indicate that in 2019, 18 highway sections experienced inundation depths ranging from 0.04 to 0.63 m for up to five months. This flooding was not caused by a single storm event but resulted from cumulative precipitation in 2018 and 2019. Using MODFLOW, we analyzed historical flooding (> 1 m increase in water level over a one- and two-year period) from 1940 to 2009 for ten highways within the NSH and model domain. Flooding frequencies ranged from 0% to 2.7% and from 1.4% to 11% for the two-year periods. These findings provide critical insights for the Nebraska Department of Transportation to prioritize highway improvement efforts in mitigating future flood risks through future construction projects to raise these highways. Observed trends in increasing precipitation, stream discharge and groundwater levels over recent decades, and their role in contributing to major flood events in 2010 and 2019, flooding risks may escalate in the future.

Contents

1. Introduction

Groundwater flooding occurs when water emerges at the surface from subsurface permeable strata, often at multiple diffuse locations (Cobby et al., 2009; Macdonald et al., 2008). This phenomenon is typically triggered by a rising water table, particularly in unconfined and shallow aquifers, due to heavy precipitation, snowmelt or a combination of both (Macdonald et al., 2008). The prolonged nature of groundwater flooding can result in significant infrastructure damage and disruption of essential services, leading to substantial socioeconomic losses (Kreibich and Thieken, 2008; Morris et al., 2018). In England, financial losses from groundwater flooding were found to be 2.5 times higher than those from overland flooding (Allocca et al., 2021). Climate change and global warming are expected to exacerbate groundwater flooding, specifically coastal communities, by altering water table levels (Pierre-Louis, 2021).

In regions with high water tables and low groundwater withdrawal rates, rising groundwater levels can transform surface water dynamics. This process can create or expand wetlands, alter surface drainage patterns, saturate soils, and inundate landscapes. Groundwater level fluctuations not only affect surface hydrology but also influence subsurface dynamics (Finch et al., 2004; Pinault et al., 2005). Unlike fluvial flooding, groundwater inundation requires more complex assessment tools and strategies (Rotzoll and Fletcher, 2012).

Remote sensing offers valuable capabilities for characterizing both surface and subsurface aspects of groundwater flooding (Becker, 2006). Satellite data can provide insights into soil moisture variability (Soylu and Bras, 2021), groundwater level fluctuations (Shrestha et al., 2021b), groundwater storage changes (Strassberg et al., 2009), inundation frequency (Ogilvie et al., 2015), and flood depth (Schumann et al., 2008). These derived datasets, when combined

with ancillary information, can help identify potential flood-prone areas. Satellite remote sensing is particularly useful for detecting both permanent and intermittent surface water inundation. Optical imagery directly estimates flooded areas but is often limited by cloud cover during flooding events. In contrast, synthetic aperture radar (SAR) can penetrate clouds and rainfall, providing accurate flood extent measurements (Amitrano et al., 2018; Schumann and Moller, 2015). SAR has been widely used in flood mapping; for instance, Tiwari et al. (2020) utilized SAR with the Otsu thresholding method to map the Kerala flood inundation area. However, SAR's effectiveness depends on factors such as wavelength, resolution, incidence angle, and polarization. Most SAR satellites operate at shorter wavelengths (<8 cm) with high incidence angles, which limits their ability to penetrate dense vegetation canopies. For example, the freely available Sentinel-1 satellite, which operates on a 5.5 cm C-band wavelength, cannot accurately detect flooding beneath vegetation (Schumann and Moller, 2015). Light detection and ranging (LIDAR) is another remote sensing tool used to derive surface water elevation, topography, and lithological features, all of which are essential for assessing flood susceptibility. In areas with shallow groundwater influencing the vadose zone, surface soil moisture data can be leveraged to characterize groundwater flooding. For instance, Ogilvie et al. (2015) combined moisture and water indices (NDMI and NDWI) to analyze flood dynamics in the Niger Inner Delta using MODIS satellite imagery. Despite advancements, most remote sensing methodologies have primarily focused on fluvial flooding, with limited applications to groundwater flooding (Aicha et al., 2020).

Groundwater modeling is another tool that can be utilized to evaluate groundwater flooding. Groundwater flooding occurs when groundwater head elevations exceed the land surface elevation. Groundwater levels are a result of many factors such as land use change, climate, and pumping rates. MODFLOW is a widely used groundwater model that simulates groundwater head. Yihdego et al. (2017) used MODFLOW-SURFACT to assess the spatial and temporal

groundwater level at a site in Australia. Mirlas et al. (2024) assessed the changes in hydrogeological conditions affecting groundwater flooding in Kazakhstan using MODFLOW.

The Nebraska Sandhills (NSH) region is particularly susceptible to groundwater flooding due to the high-water table and the large number of lakes and wetlands. Climatic factors such as rainfall and snowmelt contribute to increased moisture buildup, eventually leading to groundwater flooding. A notable example occurred in 2019 when a combination of meteorological, climatological, and hydrological events led to widespread flooding in Nebraska. A rapid cyclogenesis of an intense lee cyclone resulted in 25-50 mm of precipitation across northeastern Nebraska and 45-70 mm over central Nebraska (Flanagan et al., 2020). Concurrently, record snowfall and low surface temperatures led to rapid snowmelt, further exacerbating the flooding. This event not only triggered surface flooding but also saturated the hydrological system, leading to elevated river and groundwater levels. Numerous highways in the NSH were inundated throughout 2019 for months at a time, disrupting transportation networks. Annually, Nebraska's roadways facilitate 31.2 billion kilometers of motorist travel and transport $229 billion in commodities (National Transportation Research, 2022). From 2016 to 2021, 71% of highway water obstructions in Nebraska resulted from prolonged precipitation and ice jamming, while only 10% were attributed to groundwater flooding (National Transportation Research, 2022). Notably, 58% of all highway water obstructions occurred during the March 2019 flood, with most groundwater-induced road closures occurring in the NSH.

The authors are not aware of any studies that have used remote sensing or MODFLOW to evaluate highway inundation due to groundwater flooding. The objectives of this study are to: (1) determine the location, depth, and duration of flooded highways in the NSH using remote sensing; (2) evaluate the causes of flooding by analyzing historical precipitation data; and (3) assess the frequency of groundwater flooding using groundwater modeling.

2. Method

2.1 Study area

The NSH has an area of 50,000 km^2 and is the largest grass-stabilized dune field in the western hemisphere (Figure 1). The NSH hosts approximately 450 km^2 of shallow lakes and 4,500 km^2 of sub-irrigated meadows (Ahlbrandt and Fryberger, 1980; Smith, 1965; Gosselin et al., 2000; Sweeney and Loope, 2001). The temperature fluctuates between -40 º C in the winter to 43.3 º C in the summer. The drier western part receives 450 mm while wetter eastern area receives 690 mm of annual average precipitation (National Climatic Data Center, 2020). The existence of the large number of lakes and wetlands in the NSH is a result of the direct surface and groundwater interaction. The northern High Plains aquifer system lying underneath the NSH

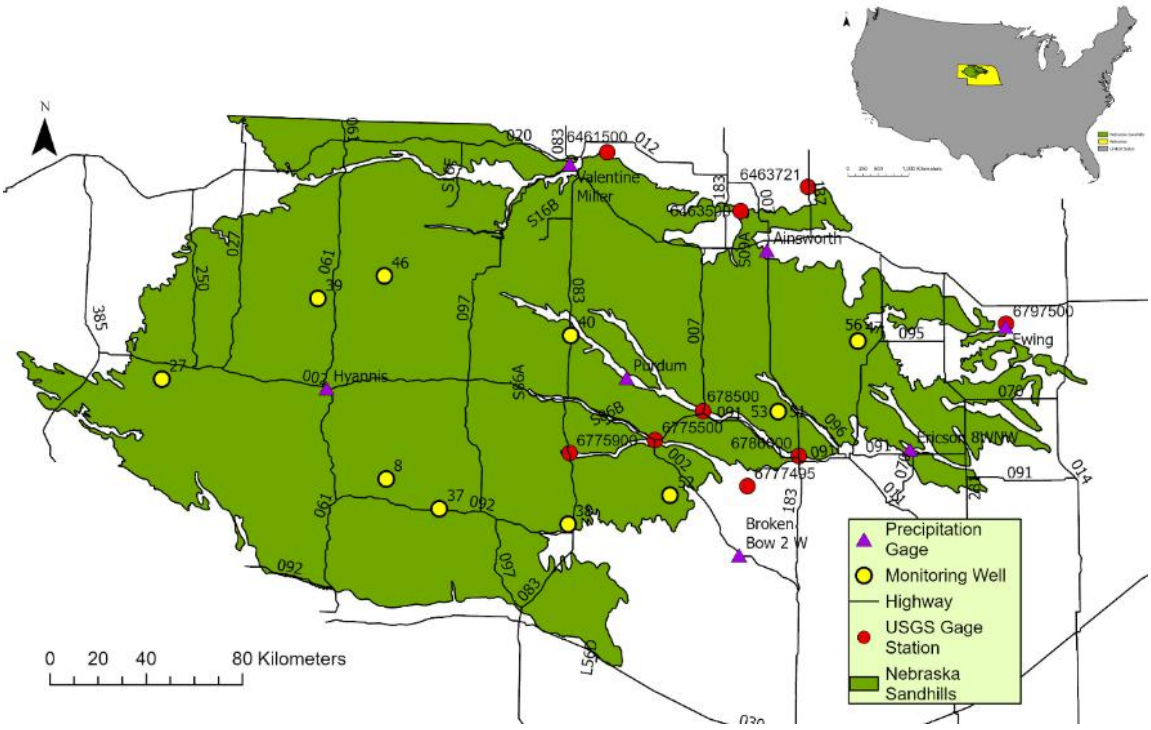

Figure 1. The Nebraska Sandhills and the location of the precipitation gages, monitoring wells, USGS gage stations, and highways.

is dominated by the Ogallala Group; a major water bearing geologic unit formed of moderate to low-permeable sand, sandstone, and siltstones deposited during the mid-Tertiary age. In NSH,

dunes of the Quaternary age overlie the unconsolidated alluvial sand, gravel, silt, and clay that overlie the Ogallala Group. The dunes, composed of very fine to medium sand, form an unconfined aquifer system serving as an important recharge area for the Ogallala aquifer (Gutentag et al., 1984; Peterson et al., 2020). The Arikaree Formation and the White River Group, which lie beneath the Ogallala Group, are also part of the High Plains aquifer, though they are finer-grained and only contain usable quantities of water locally at fractured or coarse-grained areas. In the western NSH, the Arikaree Group is underlain by the Brule Formation. This unit is composed of very fine to fine-grained sandstone with a maximum thickness of about 300 m (McGuire, 2017). Due to the fine-grained nature of the Arikaree and Brule formations, they may or may not be hydraulically connected to overlying geologic units. The Cretaceous Pierre Shale forms the impermeable base of the High Plains Aquifer in the NSH. The unconfined aquifer is directly interconnected to the Ogallala aquifer and surface water bodies such as lakes and wetlands. NSH has the greatest volume of saturated sediment in the High Plains aquifer and the least net groundwater declines (Haacker et al., 2016; McGuire, 2017; Peterson et al., 2016; Scanlon et al., 2012). They respond directly with some delay to the changes in the climate process, such as drought and deluge (Shrestha et al., 2021a).

The western and central Sandhills have minimal cropland, resulting in limited groundwater withdrawals. In contrast, the eastern Sandhills support corn cultivation, leading to greater seasonal declines in water levels during the growing season. The NSH is a highly baseflow-dominated region, with most areas exhibiting a baseflow index exceeding 90% (Szilagyi et al., 2003).

2.2 Comparison of groundwater levels and streamflow for the 2019 event

Flooding impacted central and eastern Nebraska during the 2019 storm event. To assess its effects, we analyzed groundwater levels and streamflow throughout the NSH for 2019, comparing them to historical groundwater and streamflow data. The region contains twelve real-

time monitoring wells (Real-Time Groundwater Monitoring Network, 2025) and nine USGS gage stations (U.S. Geological Survey, 2016) within or on the perimeter of the NSH (Figure 1).

For each monitoring well, the minimum and maximum groundwater levels were identified prior to and after the 2018 and 2019 precipitation events. The difference between these groundwater levels was calculated along with the time required for the groundwater to rise from minimum to peak levels.

Nine USGS gage stations within or on the perimeter of the NSH were analyzed. As shown in Figure 1, all stations are in the central and eastern parts of the NSH. The western part contains a few streams, but is home to thousands of lakes, covering 4700 km^2, most of which are less than one meter deep (Shrestha, et al., 2021). The lakes form where the groundwater level rises above the land surface.

For each USGS gage station, we calculated flow duration curves, enabling a comparison of 2019 flows against historical records. A flow duration curve illustrates the percentage of time a stream's flow is likely to equal or exceed a specific value. To construct this curve, daily discharge values were first ranked from highest to lowest. Each discharge value was then assigned a rank (M), with 1 representing the highest discharge and increasing values assigned to lower discharges. The exceedance probability (P) was determined using Equation 1:

$$P=100\times(M/n+1)$$

where:

- P is the probability that a given flow will be equaled or exceeded,
- M is the ranked position in the dataset, and
- n is the total number of daily discharge values.

2.3 Flood inundation depth and duration

Flood inundation frequency of the highways was determined using the time-series analysis of satellite images (Figure 2). We used Sentinel-2 images to derive recent (2017-2021) and past flood events in the NSH. We calculated the normalized difference moisture index (NDMI) [*NIR – SWIR)/(NIR + SWIR]* (Gao, 1996), to infer the moisture content. The NDMI provides moisture conditions due to higher groundwater levels or rainfall, or snowfall events. We used NDMI as the flood water covered by vegetation and was better represented as moisture. NDMI is sensitive to changes in vegetation water content as the amount of moisture content governs the absorbance of SWIR (MIR) band (Curran, 1989; Töyrä et al., 2002). Water indices, such as MNDWI, were not used as they likely represent the water bodies rather than the moisture level. The time-series images were then automatically threshold using the Edge Otsu threshold method. We used NDVI to mask out areas with the greenest vegetation, with the assumption that the moist vegetation tends to have lower NDVI compared to the green and dry vegetation.

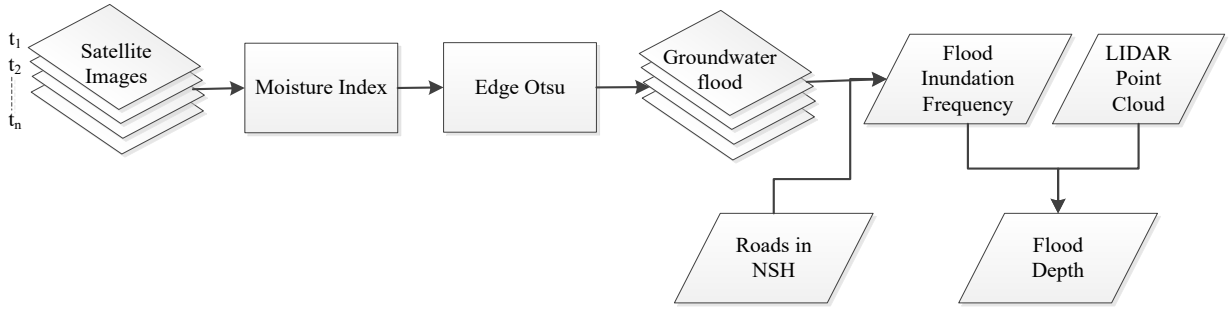

Figure 2. Flow chart to estimate the flood inundation frequency and flood depth using optical satellite images and LIDAR point clouds.

The Otsu's algorithm was implemented in the Google Earth Engine (GEE) to identify highway flooding. The Otsu's algorithm is widely used in flood mapping. This method maximizes the inter-class variance between two classes computed from a normalized image histogram. Otsu

assumes a bimodal histogram and may not provide optimal threshold when a multi-modal (more than two classes) histogram is present. The limitation is circumvented using the Edge Otsu algorithm that samples areas with a likely bimodal histogram of water/no water for optimal threshold selection. The Edge Otsu algorithm uses a Canny edge filter to extract and buffer edges of features to subsequently sample a histogram for Otsu thresholding. In this study, we used NDMI with an initial threshold of 0.2 to define the edges. The initial threshold provides binary images and alleviates the multi-modal histogram problem in the original Otsu's algorithm. The edges are filtered for smaller length to avoid small edges that can cause a skewed histogram. We used edges length and buffer of greater than 20 m to reduce misclassification. Detail on Edge Otsu algorithm is explained by Donchyts et al. (2016) and Markert et al. (2020). The threshold images were then added and divided by the number of total images to derive the flood inundation frequency for an area. Based on the flood frequency, the flood duration was inferred by manually interpreting the Sentinel-2 images.

Flood depth was derived using light detection and ranging (LIDAR) point cloud data. The LIDAR point cloud data was collected by the United States Geological Survey (USGS) in 2016, 2017, and 2020 in the NSH. The LIDAR data has an aggregate nominal pulse spacing of ≤ 0.71 m and an aggregate nominal pulse density of ≥ 2 points per m^2. The level 2 (QL2) data used in the study has an absolute vertical accuracy of ≤10 cm root mean square error (RMSE) with NAVD88 vertical datum. We downloaded the point cloud through the FTP server and used FUSION tools to clip and filter within the boundary of roads (McGaughey, 2009).

The flooded section of roads was used to extract the LIDAR point clouds. The flood inundation frequency map was converted to lines. The lines were corrected for alignment as the conversion process from raster to line results in cutbacks and other errors. We did not use polygons as the polygons overlapped beyond road sections, resulting in over- and under sampling of LIDAR points. The point clouds were then used to derive the minimum, mean, and maximum elevation

with the assumption that the flood water first fills the lowest elevation and moves to higher elevation with an increase in flood water volume. The method is similar to waterline method used to derive water elevation of lakes by Shrestha et al. (2021b).

The Nebraska Department of Transportation (NDOT) provided flood depth and/or duration data for four highways affected by flooding within the NSH. Ground measurements for the other flooded highways were not available. We compared this data to flood locations and depths derived from remote sensing. Additionally, we analyzed highway flooding locations in relation to vadose zone data.

To calculate the depth to water across the NSH, we subtracted the groundwater levels- based on 1995 water table contours- from a 30 m DEM. Using ArcGIS Pro, we identified highway locations where the water table was less than one meter below the surface. Finally, we compared these locations to flooded highways to assess the relationship between highway flooding and thin vadose zone.

2.4 Causes of 2019 flooding

To determine the cause of the 2019 flooding across the NSH, we analyzed weather data from NOAA Regional Climate Centers (xmACIS2) and identified stations within the NSH that have precipitation records dating back to the late 1800's or early 1900's, with minimal missing data (Figure 1). To evaluate 2019 precipitation events against historical data, we compared the largest storm events of 2019 to return intervals from NOAA Atlas 14 (Perica et al., 2013). Unlike flooding caused by runoff and rising stream stages, groundwater levels respond with a lag following rain events (Shrestha et al., 2021). Additionally, we evaluated cumulative annual precipitation, as well as rolling two-year and three-year precipitation totals, to better understand long-term trends.

2.5 Historical flooding in the NSH

This study employs an existing groundwater model to evaluate the extent and impact of groundwater flooding on Nebraska highways. By leveraging a previously calibrated groundwater flow model, we aim to simulate transient aquifer behavior and identify historical flooding events in the study area. The Elkhorn-Loup MODFLOW (ELM), developed by the U.S. Geological Survey (USGS), simulates groundwater flow and stream-aquifer interactions across the Elkhorn and Loup River Basins in Nebraska, covering an area of approximately 78,000 km^2. Featuring a two-layer structure and high spatial resolution, this model provides a framework for assessing historical groundwater flooding.

The model area includes the High Plains aquifer system, comprising Quaternary and Tertiary sediments, with groundwater generally flowing from west to east. The model accounts for geological variability, including glacial till in the east and the Sand Hills in the west, which influence groundwater recharge and flow patterns.

Built using MODFLOW-NWT (Niswonger et al., 2011), the model employs a three-dimensional finite-difference approach to simulate groundwater flow. It is divided into two layers: the upper layer represents the Plio-Pleistocene sediments, and the lower layer covers deeper aquifer systems. The grid structure consists of half-mile cells, totaling 235,643 active cells.

2.5.1 The model's temporal framework spans:

- A 1,000-year transient stress period for pre-1895 conditions, establishing a natural steady-state baseline.
- Two stress periods from 1895 to 1940 represent the introduction and expansion of surface water irrigation.
- Monthly transient stress periods from 1940 to 2009, capturing groundwater use during this era.

Calibration was performed to represent historical conditions. Over 150,000 groundwater-level observations and 22,169 monthly base-flow targets from 51 stream gages were used. Parameters such as hydraulic conductivity, specific yield, and recharge rates were refined using both manual adjustments and automated parameter estimation with PEST software. Recharge was estimated using the Soil-Water Balance (SWB) model, incorporating precipitation, irrigation, and canal seepage. Stream-aquifer interactions were modeled using the Streamflow Routing (SFR2) package, which accounted for streambed conductivity, width, and the effects of pumping on base flows.

For the transient period from 1940 to 2009, the model outputs, directly run by the USGS, were used to analyze the simulated groundwater levels. These outputs were post-processed to evaluate historical flooding at predefined highway areas in Nebraska during this period.

2.5.2 Uncertainty Evaluation of the Elkhorn-Loup Groundwater Model

Groundwater models inherently contain uncertainties due to limitations in input data, assumptions in model design, and the scale at which the system is represented. The Elkhorn-Loup groundwater model, constructed with a horizontal grid resolution of 0.5-mile (approximately 800 meters) and two vertical layers, was calibrated using a large dataset of groundwater level observations and stream baseflow targets to reduce uncertainty. However, despite extensive calibration, variations exist between simulated and observed values, which must be considered when interpreting model results.

2.5.3 Groundwater Level Uncertainty (1940–2010)

For the 1940–2010 transient simulation, the model was calibrated using 149,902 groundwater level measurements, with a mean residual of -0.77 m and a median residual of -1.0 m. The standard deviation of the residuals was 5.0 m, meaning that while the model provides a reasonable regional approximation, local deviations can be significant. About 75 percent of the

simulated groundwater levels were within 4.6 feet of the observed values, but localized errors may exceed this range.

These discrepancies arise from several factors. The simplification of aquifer properties within each 800-meter grid cell leads to a loss of local-scale variability in hydraulic conductivity, recharge, and boundary conditions. Additionally, the accuracy of historical groundwater level measurements varies, as older datasets may lack detailed records of measurement conditions, though observations were weighted based on measurement uncertainty. The use of spatially averaged parameters also limits the model's ability to capture highly localized groundwater fluctuations, particularly in areas where small-scale hydrogeologic features influence groundwater flow.

2.5.4 Comparison of Simulated Heads with Highway Elevation Data

To further evaluate model uncertainty at highway locations, simulated groundwater heads for specific highway cells, based on remote sensing analysis and NDOT provided highway locations, were compared with the minimum and maximum elevation values derived from a 1-meter resolution Digital Elevation Model (DEM) from the USGS 3D Elevation Program (3DEP). The comparison provides a way to assess whether simulated groundwater levels indicate potential flooding conditions at specific road segments. The 1-meter DEM captures finer-scale topographic variations that are not represented in the model's 800-meter grid resolution, offering additional insights into the potential for localized groundwater emergence. However, since the model operates at a coarser resolution, there may be cases where small-scale depressions or elevation changes affect flooding risk in ways that the model does not fully capture.

We analyzed each flooded highway using the ELM model for the period 1940–2009, simulating groundwater levels on a monthly basis. At each location, the simulated groundwater head was near or above the lowest elevation of the corresponding model cell, except for Highway 16F.

This highway is located in the northern section of the model, where boundary conditions create significant uncertainty (USGS, 2008). Here, the simulated groundwater head was nearly 10 meters below the lowest elevation in the model cell, so we excluded it from further analysis.

For the remaining flooded highway locations within the model domain (Highways 61, 97, 83, and 183), we calculated the change in elevation between the current and previous month. We then summed these differences over one-year and two-year periods. If the change in elevation exceeded one meter, we assumed the highway was flooded.

The comparison of simulated heads with high-resolution DEM data from the USGS 3DEP improves the evaluation of flood-prone areas along highways, although finer-scale modeling may be needed for precise local flood predictions. Understanding the limitations of the model allows for better interpretation of results and more informed decision-making in groundwater management and infrastructure planning.

3. Results

3.1 Comparison of groundwater levels and streamflow for the 2019 event

Groundwater levels in the 12 monitoring wells within the NSH rose between 0.52 to 2.79 m during the 2017-2020 time period (Table 1). The lowest water levels prior to the groundwater level increase were in 2017 and 2018. For instance, in September 2017, the water level in well number 40 was 1.88 m below ground level. The level continued to rise, eventually peaking at 0.57 m in June 2020 (Figure 3). Most wells reached their highest levels in 2019 or 2020, except for wells 39 and 53, both deep wells. However, well 56, despite being deep, peaked earlier in 2019. Southeastern NSH experienced the greatest increase in water levels, whereas the western NSH saw the smallest rise. The western-most well (#27) only increased by 0.65 m, while the easternmost well (#56) rose by 1.23 m. Notably, well 52 saw a sharp increase of 2.79 m in only six months.

Table 1. Water levels in wells prior to above-average precipitation from 2017 to 2019, the peak water level in 2019 or 2020 and the total increase in water levels.

Well ID	Water level prior to 2019 increase (m) (Date)	Peak water level (m) (Date)	Increase in water level (m)
8	4.31 (October 9, 2017)	3.63 (May 4, 2020)	0.68
27	1.43 (April 10, 2018)	0.78 (June 16, 2020)	0.65
37	1.66 (October 3, 2018)	0.77 (May 28, 2019)	0.89
38	1.71 (Sept. 16, 2017)	0.10 (June 14, 2020)	1.33
39	5.16 (April 2, 2019)	4.46 (March 2, 2022)	0.70
40	1.88 (Sept. 17, 2017)	0.57 (June 10, 2020)	1.31
46	0.72 (Sept. 18, 2018)	0.20 (March 19, 2020)	0.52
47	2.25 (July 26, 2017)	0.66 (Dec. 28, 2019)	1.59
51	2.52 (August 19, 2017)	0.57 (May 25, 2020)	1.95
52	4.74 (March 15, 2019)	1.38 (Sept. 17, 2019)	2.79
53	25.45 (April 19, 2018)	23.59 (April 29, 2022)	1.81
56	11.60 (July 23, 2017)	10.37 (Dec. 23, 2019)	1.23

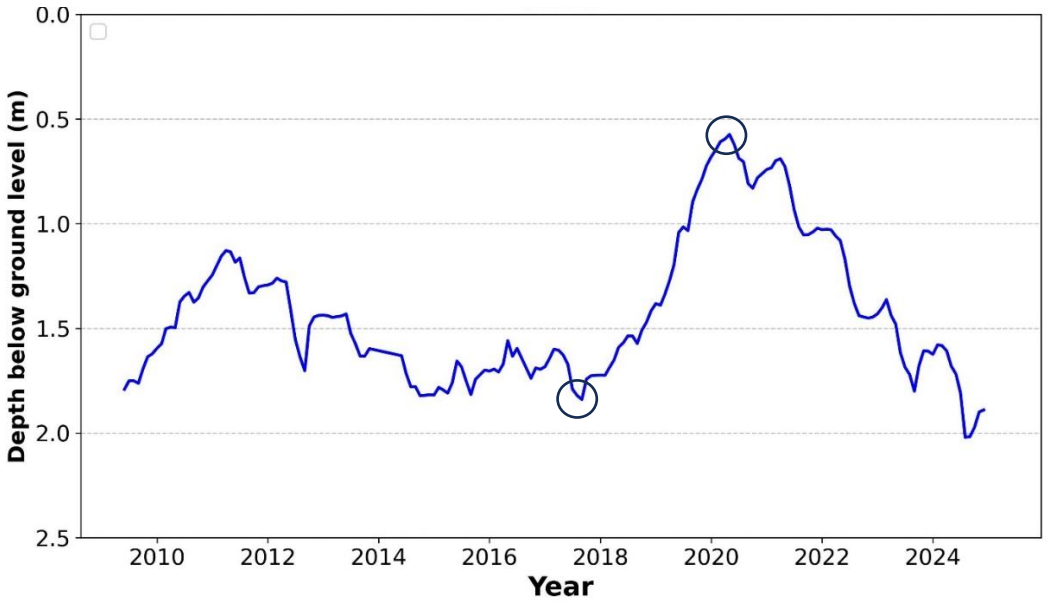

Figure 3. Average monthly water depth from 2009 to 2024 at monitoring well number 40.

Among the nine stream gages, the maximum flow occurred in March 2019 for four gages and June 2010 for four gages (Table 2). Dismal River gage station (6775900) exhibited an unusual peak in 1983, deviating from its typically stable hydrograph, which generally ranges from 4 and 10 m^3s^{-1}. Figure 3 further highlights the increasing trend in streamflow, which will be explored

later in the discussion. Flow duration curve calculations indicate that 2019 flows ranked in the top 0.2% of the historic measurements.

Table 2: Summary of streamflow data for the nine USGS gauge stations within or near the Nebraska Sandhills. The summary includes the period of record with missing data in parenthesis, minimum, average and maximum streamflow and the flow duration results for the 2019 flood event. (*years of missing data)

USGS Station	Period of Record*	Minimum Streamflow (m^3s^{-1})	Mean Streamflow (m^3s^{-1})	Maximum Streamflow (m^3s^{-1}) and Date	Flow Duration Curve (2019)
6775900	1966-current (5)	3.54	6.13	13.10 (Aug. 1983)	0.14 (May 22, 2019: 8.86 m^3s^{-1})
6775500	1965-current (5)	4.79	13.18	25.69 (June 2010)	0.01 (May 28, 2019: 25.10 m^3s^{-1})
6785500	1945-current (59)	3.37	13.64	99.99 (June 2010)	0.09 (May 22, 2019: 59.43 m^3s^{-1})
6777495	2017-current	12.68	30.29	64.24 (Mar. 2019)	0.04 (March 13, 2019: 64.24 m^3s^{-1})
6786000	1936-current	1.27	14.71	143.8 (June 2010)	0.02 (May 24, 2019: 86.32 m^3s^{-1})
6463500	1948-current (1)	1.25	4.76	133.6 (Mar. 2019)	0.04 (Mar. 14, 2019): 133.6 m^3s^{-1}
6461500	1945-current	2.83	22.49	163.0 (Mar. 2019)	0.00 (Mar. 25, 2019: 163.0 m^3s^{-1})
6463720	2012-current	8.86	43.96	549.0 (Mar. 2019)	0.02 (Mar. 14, 2019: 549.0 m^3s^{-1})
6797500	1947-current	0.13	6.19	713.2 (June 2010)	0.03 (Mar. 18, 2019: 217.9 m^3s^{-1})

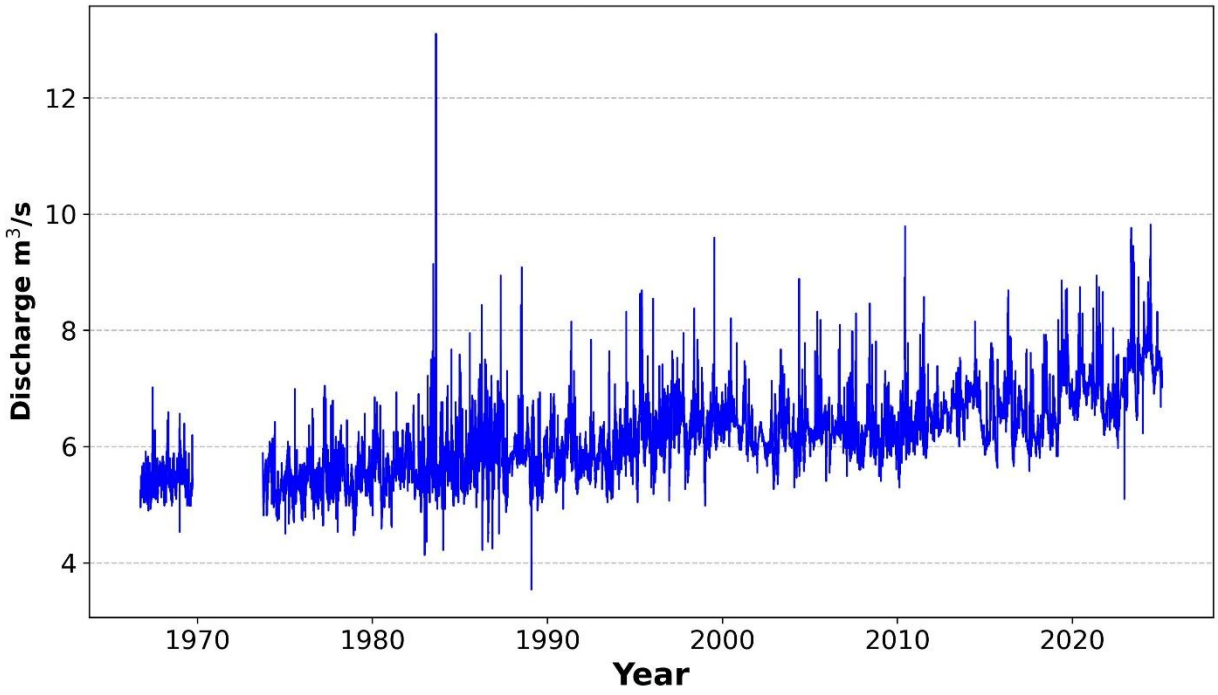

Figure 4. Discharge from 1965 to 2024 on the Dismal River in the western Nebraska Sandhills.

3.2 Flood depth

We first calculated the depth of flooding for each highway within the NSH and compared these depths with data collected by NDOT. An elevation profile along the flooded highway demonstrates that LiDAR and high-resolution digital elevation models provide accurate estimates of floodwater depth. The central portion of the road, which is most frequently flooded, exhibits little variation in elevation, whereas the boundaries of the flooded road show greater variation. Highways passing through wetlands experience the most frequent inundation, with flooding primarily concentrated in the center of the roads.

To estimate flood depth for inundated highways, we calculated the difference between the minimum and maximum elevations. Our analysis covered nine highways, moving from west to east: Highways 250, 27, 61, 2, 16, 97, 83, 40, and 183. Of these, NDOT documented flooding

on four highways: 61, 97, 83, and 183. **Error! Reference source not found.** indicates that measured flood depths ranged from 4 to 63 cm.

For each of the four highways that NDOT reported flooding, our remote sensing methodology also measured flooding. The flood depths reported by NDOT are not directly comparable to our measurements, as the Sentinel image we used may not coincide exactly with the dates of NDOT's observations. The flooding depths using LIDAR compared very well for highways 61_2 and 83_1. Overall, these results demonstrate that highway flood inundation depth can be effectively estimated using LiDAR data.

Table 3: Flood depth of major highways estimated using LIDAR data and ground-measured depths for four locations.

Highway Location Name	Z Minimum (m)	Z Maximum (m)	Depth (m)	Ground-measured depth (m)
250_1	1161.07	1161.12	0.05	
250_2	1182.98	1183.12	0.14	
27_1	1176.25	1176.38	0.13	
27_2	1192.95	1193.04	0.09	
27_3	1193.40	1193.44	0.04	
61_1	1132.64	1132.68	0.04	
61_2	1132.29	1132.49	0.20	0.15-0.20
16F_1	911.62	911.67	0.05	
16F_2	920.83	920.98	0.15	
16F_3	930.39	930.84	0.45	
97_1	918.76	919.04	0.28	0.91
97_2	936.26	936.30	0.04	
97_3	936.17	936.32	0.15	
83_1	893.54	893.66	0.12	0.15-0.20
83_2	864.93	864.97	0.04	
83_3	887.40	887.46	0.06	
183	771.63	772.26	0.63	0.10
2	881.71	881.83	0.12	

3.3 Flood inundation duration

The duration of flooding was estimated through visual interpretation of Sentinel-2 images for five major highways: 27, 16F, 97, 83, and 183 (Table 4). The results indicate that most inundated highways remained flooded for over a month in 2019. Notably, State Highway 16F_2 also experienced flooding in 2020. The majority of flooding occurred between June and November 2019.

NDOT reported flooding duration for highways 97, 83, and 183. On June 6th, NDOT reported that Highway 97_1 had 0.91 meters of water covering the roadway. Water was pumped from the highway to Merritt Reservoir starting on June 23rd. Pumping was completed by August 1st. These dates closely align with the flood duration estimated using Sentinel imagery, which ranged from May 31 to August 9. For Highway 83, NDOT reported flooding all summer/fall with the highway open to 2-way traffic on November 14th, 2019, which also aligns well with Sentinel-based calculations (May 31 to November 17). Meanwhile, NDOT noted that a section of Highway 183 near Rose, NE, had water over the roadway from September 23rd to October 7th. However, Sentinel imagery detected flooding for only five days in mid-September.

Overall, remote sensing provided reliable estimates for the duration of highway flooding, demonstrating its effectiveness in monitoring flood events.

Table 4: Flood duration of major highways in the Nebraska Sandhills from 2015-2020 calculated using remote sensing.

Road Name	Start Date	End Date	Duration	Start Date	End Date	Duration
State HW 27_1	6/3/2019	7/28/2019	1 m 25 d	8/17/2019	8/27/2019	10 d
State S 16F_2	5/31/2019	9/26/2019	3 m 26 d	5/5/2020	6/4/2020	30 d
State S 16F_3	5/31/2019	6/3/2019	3 d	-	-	-
State HW 97_1	5/31/2019	8/9/2019	2 m 9 d	-	-	-
State HW 97_2	5/31/2019	10/18/2019	4 m 18 d	-	-	-
State HW 83_1	5/31/2019	11/17/2019	5 m 17 d	-	-	-

US HW 183	9/13/2019	9/18/2019	5 d	-	-	-

3.4 Highway flooding locations compared to water table depths

The thickness of the vadose zone was calculated by taking the difference from the 30-m digital elevation model and the spring 1995 water table digital data (Figure 5). The vadose zone depths ranged from 0 to 131 m. Of the total 47,535 km^2 within the NSH, 1,052 km^2 are lakes and wetlands and 829 km^2 have a vadose zone thickness of less than one meter. There are 63 locations where a highway intersects those locations with a vadose zone thickness of less than one meter. These locations, not surprisingly, are in similar locations as the ones that flooded (**Error! Reference source not found.**).

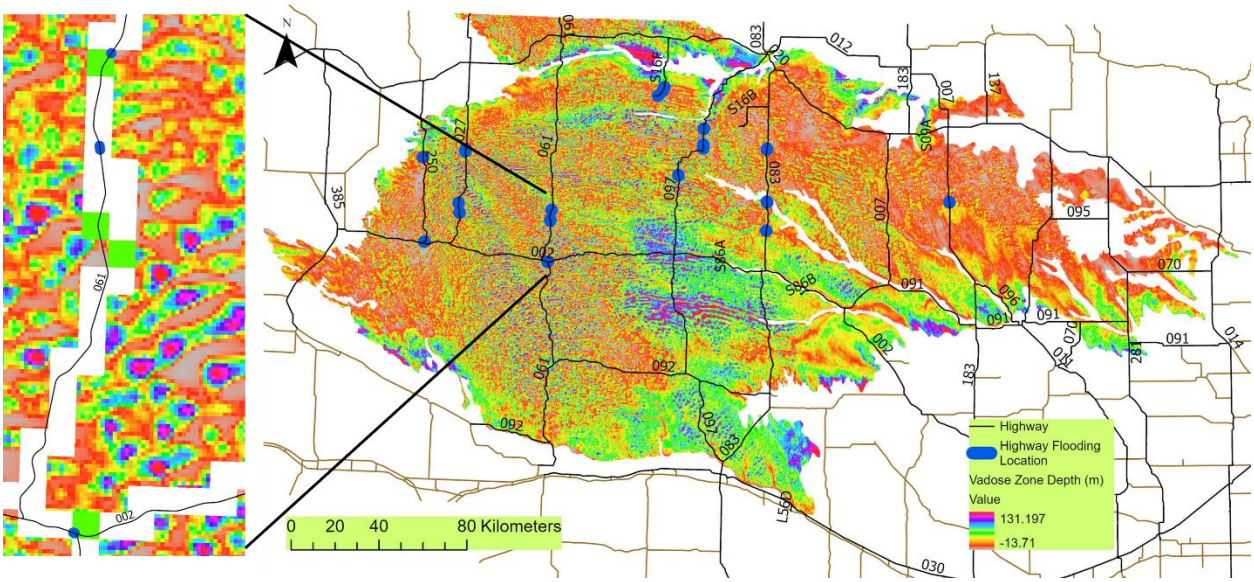

Figure 5. Image on the left illustrates a zoomed in section of highway 61. The green squares illustrate locations where the water depth is less than one meter and intersect the highway. The locations are right on or close to the flooded locations identified using remote sensing.

3.5 Causes of highway flooding

Table 5 summarizes precipitation data from stations within NSH for the 2019 event, comparing it to recurrence intervals derived from NOAA Atlas 14 data for a 24-hour storm. The reported precipitation represents the maximum value recorded at each station in 2019. Most stations experienced maximum precipitation below the 2-year recurrence interval, while rainfall at the

Purdum and Ainsworth stations fell between the 5- to 10-year and 10- to 25-year recurrence intervals, respectively.

Groundwater flooding exhibits lag time and cumulative precipitation impacts. Figure 6 presents historical precipitation data for the Purdum and Hyannis stations, both near highways affected by the 2019 flooding. Figures (A), (B), and (C) display annual total precipitation, 2-year cumulative precipitation, and 3-year cumulative precipitation, respectively. At Purdum, 2019 (A), 2018–2019 (B), and 2017–2019 (C) show significantly higher precipitation than any other period. At Hyannis, 2018–2019 recorded the highest two-year precipitation total, whereas 2008–2010 had the highest three-year total. Other NSH stations also exhibit similar trends, with 2019 being a notably wetter period compared to previous consecutive years.

Table 5: Comparison of the maximum precipitation event in 2019 at six climate stations and the precipitation amounts for 2-yr to 100-yr return periods.

	Precipitation (mm)	**NOAA Atlas 14 24-hour storm (mm) for different return periods**						**Precipitation return period comparison**
NOAA station	**Maximum**	**2-yr**	**5-yr**	**10-yr**	**25-yr**	**50-yr**	**100-yr**	
Ainsworth	92	58	74	87	104	119	133	Between 10-yr and 25-yr
Ericson	46	61	79	94	115	132	150	< 2-yr
Ewing	34	69	89	105	125	142	159	< 2-yr
Hyannis	33	52	68	81	98	113	128	< 2-yr
Purdum	78	57	74	87	105	118	132	Between 5 - yr and 10-yr
Valentine	46	55	70	82	99	113	127	<2-yr

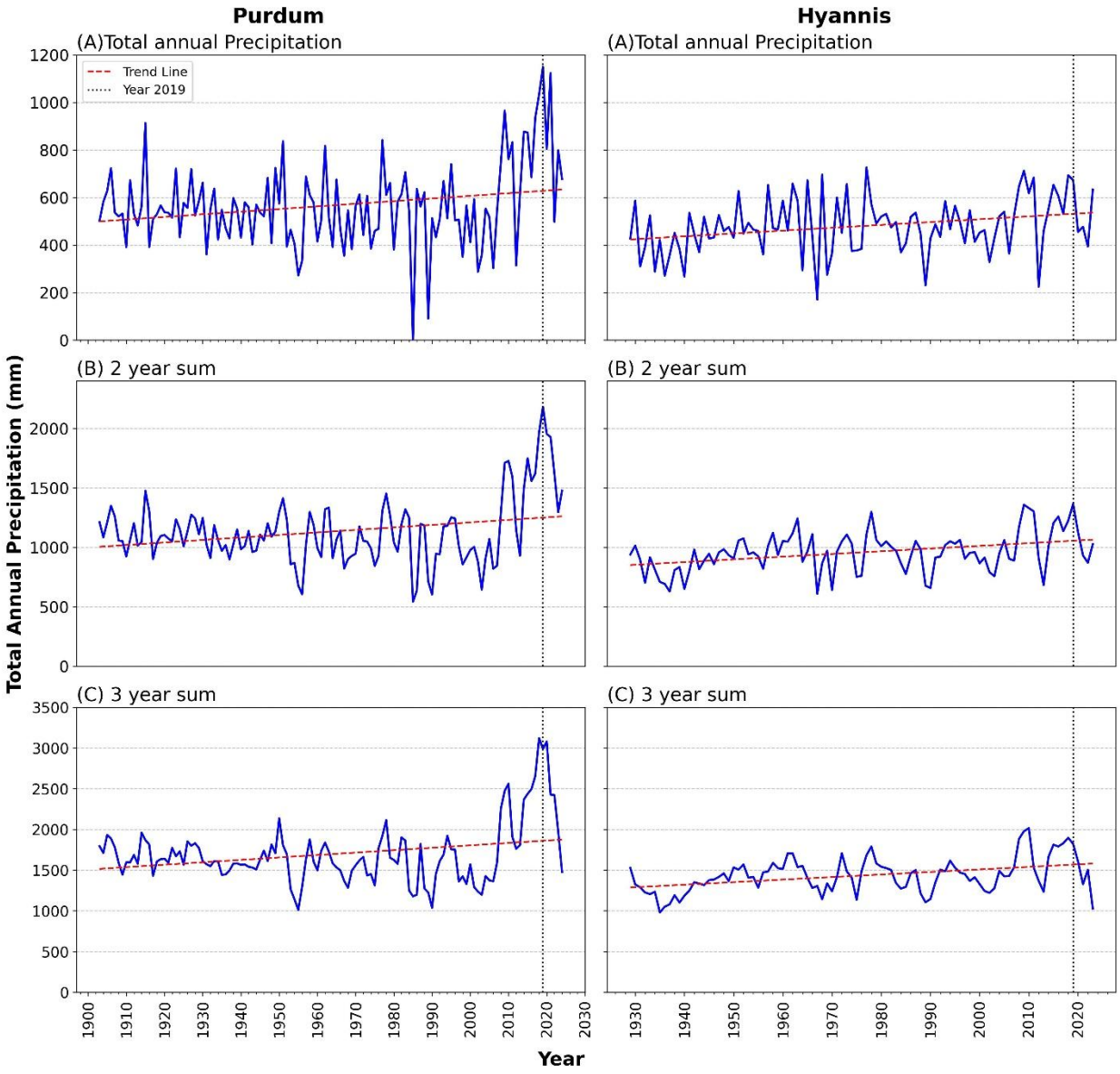

Figure 6. Total annual precipitation, 2-year sum, and 3-year sum cumulative precipitation for (I) Prudum and (II) Hyannis stations

3.6 Frequency of highway flooding

Although highway flooding was documented between 2018 and 2020, we aimed to determine historical flooding patterns using MODFLOW from 1940 to 2009 and assess the frequency of

highway inundation. We assumed that if the groundwater level increased by one meter over a one-year or two-year period, flooding occurred.

The analysis showed that the frequency of flooding within a one-year period ranged from 0% to 2.7%, while the frequency of flooding over a two-year period varied between 1.4% and 11.3%. The most significant flooding occurred in the early 1940s and 1980s. Additionally, Highway 183 experienced flooding in the mid-1960s, early 1970s, 1990s, and 2007–2008, while Highway 97 was affected between 2007 and 2009. The groundwater level increased from 2007 to 2009 ultimately contributed to the flooding observed in 2010. While model limitations prevent us from determining exact flooding frequencies, the data provides insight into historical flooding patterns and the precipitation events that triggered them.

Figure 7 presents the average two-year precipitation totals for all weather stations. Each significant groundwater rise of one meter corresponds with increased precipitation, except in the early 1940s. This discrepancy may be due to the model's limited warm-up period, as simulations began in 1940. The highest recorded precipitation periods were 2018–2019 (1,719 mm), 2017–2018 (1,540 mm), and 2019–2020 (1,443 mm). The years 2007–2008 (1,440 mm), 2008–2009 (1,376 mm), and 2009–2010 (1,336 mm) ranked 4th, 10th, and 15th, respectively. Similarly, the periods 1978–1979 and 1983–1984 ranked 10th and 15th, contributing to flooding in the early 1980s.

Before 1940, three notable periods of potential flooding were identified: 1905–1906 (1,439 mm, ranked 5th), 1891–1892 (1,415 mm, ranked 6th), and 1914–1915 (1,359 mm, ranked 12th). Notably, the 2018–2019 period was considerably wetter than any other recorded time frame, likely resulting in the most significant flooding since the late 1890s. Other high-precipitation events likely led to less severe flooding.

Table 6. The percentage and times when the water level increased by at least one meter over a one and two-year periods.

Highway	1 yr	2 yr
61_1	0%	2.0% (1982-1983)
61_2	0%	1.4% (1982-1983)
61_3	0%	1.3% (1980-1981)
97_1	1.9% (1941-1942; 1982-1983)	3.7% (1981-1984)
97_2	1.3% (1982-1983)	4.0 (1941; 1981-1984; 2007-2009)
97_3	2.1% (1941-1942; 1982-1983)	5.7% (1941-1943; 1966; 1981-1984)
83_1	0%	1.4% (1982-1983)
83_2	0.4% (1982-1983)	1.5 (1982-1983)
83_3	1.4% (1982-1983)	5.1% (1941; 1981-1984; 2009-2010)
183	2.7% (1965; 1982-1983)	11.3% (1964-1966; 1972-1973; 1981-1984; 1991-1996; 2007-2008)

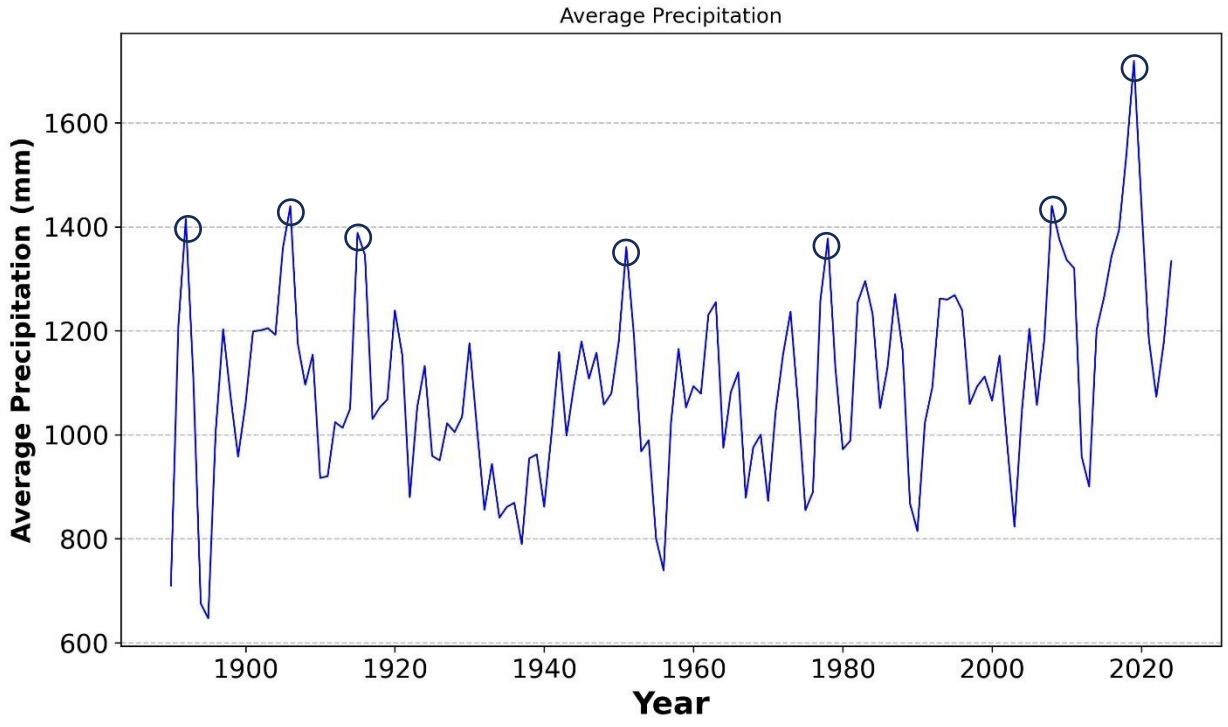

Figure 7. The average precipitation for the seven rain gages across the Nebraska Sandhills.

4. Discussion

The flood inundation frequency, duration, and depth of highway flooding were efficiently mapped using satellite data. The method shows potential for the application of remote sensing images to analyze and map groundwater flooding. The Sentinel-2 images provide the spatial and temporal representation of highway flood inundation at high spatial (10/20 m) and temporal (5/10 days) resolution, while LIDAR data provide accurate estimates of flood depth. One of the challenges of using optical satellite images for inundation mapping is the presence of cloud during flooding events. However, most of the groundwater flooding occurs after the initial onset of precipitation events due to delayed response from subsurface processes. The inundated highways showed a spatial pattern in flood frequency. Sections lying lower were most frequently inundated, while sections higher were least inundated. The results also highlight that the NDMI can quantify moisture content of vegetation and be applied to assess the flood inundation due to groundwater flooding. Although water-based indices are widely used to estimate the flood inundation area, they are insensitive when the flood water level is low or when there is a higher amount of backscatter from background. Studies mainly use SAR satellites to compensate for periods with cloud cover. However, freely available SAR sensors use shorter wavelength or have coarse spatial resolution that are unsuitable to characterize the inundation under vegetation. With the possible launch of NASA-ISRO satellite mission (NISAR), ESA-BIOMASS, the future of SAR in groundwater flood assessment is tremendous.

Using MODFLOW, the frequency of flooding since the 1940's was analyzed. We found that highway 183 followed by highways 97_3 and 83_3 flooded the most during this time period. This analysis helps the Nebraska Department of Transportation prioritize highways that may need elevation adjustments to mitigate future flooding risks. With a finite amount of funds for highway improvements, there is a need to prioritize any highway construction. The flood depths calculated using LIDAR can be utilized to determine the amount the highways need to be

raised. For example, highway 83 flooded by 0.63 m so will need to be raised a significant amount vs highways 97_3 and 83_3 were only inundated by 0.15 and 0.06 meters of water.

In our study, the cumulative effects of precipitation over multiple years, rather than a single extreme event, were found to be a key driver of groundwater flooding in the NSH region. The observed precipitation at the Prudum and Ainsworth stations suggests that flooding across NSH was not caused by a single event but rather by cumulative precipitation effects. Furthermore, the substantially higher precipitation observed at Prudum in 2019, 2018-2019, and 2017-2019 suggests that these periods could potentially contribute to an increase in groundwater levels. Similarly, the highest 2-year total precipitation at Hyannis in 2018-2019 and highest 2-year total precipitation in 2008-2010 demonstrate that the cumulative precipitation could have led to groundwater flooding. These findings align with streamflow data indicating that 2010 and 2019 were historically significant flood years in NSH. The observed lag between precipitation and flooding supports the concept that groundwater flooding develops over time, as a result of the cumulative effects of precipitation over several years.

Although 2018-2019 precipitation levels were the highest on record, flooding may be attributed to a long-term increase in precipitation (Figures 7, 8), streamflow (Figure 4) and groundwater levels over the past century. Since the 1980's, groundwater head has increased significantly across much of the NSH, rising between one and four meters (Groundwater-Level Changes in Nebraska, 2023). Chen et al (2003) evaluated streamflow and precipitation trends throughout the NSH from 1976 to 1998, finding that discharge in the Dismal, Middle Loup, North Loup and Cedar, had increasing discharge with slopes ranging from 1.24 to 4.76. Since 1895, the increased trend in precipitation has had a slope of 1.81 (Figure 7).

The12 monitoring wells located within the NSH can be used as a tool for predicting when future flooding may occur. For example, well #40, located near Highway 83, could be used to predict when future flooding may occur along the highway. The water level increased by 1.31 m in well

#40 from 2017 to 2020 and by 0.12, 0.04 and 0.06 m at three locations along Highway 83. In the future, when the water level increases approach 1.10 m, this can be an early indicator that flooding may occur along Highway 83 sometime over the next year.

The results could potentially be used to derive the vulnerability index for highways. A road passing closer to high inundation frequency with proper environmental conditions (e.g., gentle slope) could be vulnerable to future groundwater flooding. The flood inundation frequency and depth could also be used to evaluate the condition necessary for groundwater flooding. With supplementary antecedent soil moisture, precipitation, elevation, and other ancillary information, a simple lumped model, a complex groundwater models, machine learning or statistical models could be developed to understand and predict the current and future flooding states.

5. Conclusion

In conclusion, the 2019 flooding event in the Nebraska Sandhills (NSH) was a complex hydrologic occurrence influenced by both surface and subsurface water dynamics. Groundwater levels rose significantly across the region, with increases between 0.52 and 2.79 meters recorded at 12 monitoring wells. The southeastern NSH experienced the largest rises, particularly at well 52, which showed a rapid increase of 2.79 meters in six months. These groundwater surges corresponded with historic streamflow peaks, as demonstrated by USGS data showing 2019 flows ranking among the highest on record—often in the top 0.2% of historic measurements. The extent and depth of highway flooding were effectively mapped using LiDAR and remote sensing tools. Flood depths across affected highways ranged from 4 to 63 cm, with roads traversing wetland areas being particularly vulnerable. Highways 61, 97, 83, and 183, as documented by NDOT and validated through satellite imagery, experienced prolonged inundation—often lasting over a month and, in some cases, nearly half a year. This

demonstrates that remote sensing not only aligns well with ground-based observations but also provides valuable insights into flood dynamics over time and space. The spatial relationship between shallow vadose zones (less than one meter thick) and flooded highways further confirmed the role of elevated groundwater tables in the 2019 flood event. Out of 47,535 km² in the NSH, about 829 km² have such shallow vadose zones, intersecting highways at 63 locations that closely matched the flooded sites. This suggests that groundwater, rather than extreme short-term rainfall alone, played a central role in highway flooding. Precipitation analysis reinforced this finding. While daily rainfall extremes in 2019 were generally below the 2-year return interval at most stations, cumulative precipitation over two to three years reached unprecedented levels. For instance, cumulative precipitation at Purdum and Hyannis stations from 2017-2019 far exceeded historical records. This multi-year wet period saturated the landscape, leading to elevated groundwater tables that, combined with relatively modest daily rainfalls, caused widespread flooding. Historical analysis of groundwater rise frequencies between 1940 and 2009 showed that similar flooding mechanisms have occurred in past wet periods, notably in the early 1940s, 1980s, and late 2000s. The 2018-2019 period, however, emerged as the wettest on record, surpassing even the high-precipitation years of the late 18th century, thus explaining the severity and extent of the 2019 flood event. Overall, this study demonstrates that the 2019 NSH flooding was predominantly a groundwater-driven event, exacerbated by sustained multi-year precipitation. Remote sensing and elevation data proved effective for monitoring flood extent, depth, and duration, offering valuable tools for future flood management. Understanding the interaction between precipitation, groundwater response, and infrastructure vulnerability is crucial for mitigating the impacts of such floods in this sensitive sandhills environment.

6. Reference

Ahlbrandt, T.S., Fryberger, S.G., 1980. Eolian deposits in the Nebraska sand hills. US Geol. Surv. Prof. Pap. 1120, 1–24.

Aicha, O. Abdessamad, G. Hassane, J.O. Groundwater Flooding in Urban Areas: Occurrence process, Potential Impacts and The Role Of Remote Sensing And GIS Techniques In Preventing It. *2020 IEEE International conference of Moroccan Geomatics (Morgeo)*, Casablanca, Morocco, 2020, pp. 1-5, doi: 10.1109/Morgeo49228.2020.9121879.

Allocca, V., Di Napoli, M., Coda, S., Carotenuto, F., Calcaterra, D., Di Martire, D., De Vita, P., 2021. A novel methodology for Groundwater Flooding Susceptibility assessment through Machine Learning techniques in a mixed-land use aquifer. Sci. Total Environ. 790, 148067. https://doi.org/10.1016/j.scitotenv.2021.148067

Amitrano, D., Di Martino, G., Iodice, A., Riccio, D., Ruello, G., 2018. Unsupervised Rapid Flood Mapping Using Sentinel-1 GRD SAR Images. IEEE Trans. Geosci. Remote Sens. 56, 3290–3299. https://doi.org/10.1109/TGRS.2018.2797536

Ascott, M.J., Marchant, B.P., Macdonald, D., McKenzie, A.A., Bloomfield, J.P., 2017. Improved understanding of spatio-temporal controls on regional scale groundwater flooding using hydrograph analysis and impulse response functions. Hydrol. Process. 31, 4586–4599. https://doi.org/10.1002/HYP.11380

Becker, M.W., 2006. Potential for Satellite Remote Sensing of Ground Water. Groundwater 44, 306–318. https://doi.org/10.1111/J.1745-6584.2005.00123.X

Chen, X., Chen, X., Rowe, C., Hu, Q., Anderson, M., 2003. Geological and climatic controls on streamflows in the Nebraska Sand Hills. J. Am. Water Resourc. Assoc. 39(1):217-228.

Cobby, D., Morris, S., Parkes, A., Robinson, V., 2009. Groundwater flood risk management: advances towards meeting the requirements of the EU floods directive. J. Flood Risk Manag. 2, 111–119. https://doi.org/10.1111/J.1753-318X.2009.01025.X

Collins, S.L., Christelis, V., Jackson, C.R., Mansour, M.M., Macdonald, D.M.J., Barkwith, A.K.A.P., 2020. Towards integrated flood inundation modelling in groundwater-dominated catchments. J. Hydrol. 591, 125755. https://doi.org/10.1016/J.JHYDROL.2020.125755

Colombo, L., Gattinoni, P., Scesi, L., 2018. Stochastic modelling of groundwater flow for hazard assessment along the underground infrastructures in Milan (northern Italy). Tunn. Undergr.

Sp. Technol. 79, 110–120. https://doi.org/10.1016/J.TUST.2018.05.007

Curran, P.J., 1989. Remote sensing of foliar chemistry. Remote Sens. Environ. 30, 271–278. https://doi.org/10.1016/0034-4257(89)90069-2

Donchyts, G., Schellekens, J., Winsemius, H., Eisemann, E., van de Giesen, N., 2016. A 30 m Resolution Surface Water Mask Including Estimation of Positional and Thematic Differences Using Landsat 8, SRTM and OpenStreetMap: A Case Study in the Murray-Darling Basin, Australia. Remote Sens. 2016, Vol. 8, Page 386 8, 386. https://doi.org/10.3390/RS8050386

Finch, J.W., Bradford, R.B., Hudson, J.A., 2004. The spatial distribution of groundwater flooding in a chalk catchment in southern England. Hydrol. Process. 18, 959–971. https://doi.org/10.1002/HYP.1340

Flanagan, P.X., Mahmood, R., Umphlett, N.A., Haacker, E., Ray, C., Sorensen, W., Shulski, M., Stiles, C.J., Pearson, D., Fajman, P., 2020. A Hydrometeorological Assessment of the Historic 2019 Flood of Nebraska, Iowa, and South Dakota. Bull. Am. Meteorol. Soc. 101, E817–E829. https://doi.org/10.1175/BAMS-D-19-0101.1

Fürst, J., Bichler, A., Konecny, F., 2015. Regional Frequency Analysis of Extreme Groundwater Levels. Groundwater 53, 414–423. https://doi.org/10.1111/GWAT.12223

Gao, B.C., 1996. NDWI—A normalized difference water index for remote sensing of vegetation liquid water from space. Remote Sens. Environ. 58, 257–266. https://doi.org/10.1016/S0034-4257(96)00067-3

Gutentag, E.D., Heimes, F.J., Krothe, N.C., Luckey, R.R., Weeks, J.B., 1984. Geohydrology of the High Plains aquifer in parts of Colorado, Kansas, Nebraska, New Mexico, Oklahoma, South Dakota, Texas, and Wyoming (USGS, USA, groundwater). US Geol. Surv. Prof. Pap. https://doi.org/10.3133/pp1400B

Haacker, E.M.K., Kendall, A.D., Hyndman, D.W., 2016. Water Level Declines in the High Plains Aquifer: Predevelopment to Resource Senescence. Groundwater 54, 231–242. https://doi.org/10.1111/gwat.12350

Habel, S., Fletcher, C.H., Rotzoll, K., El-Kadi, A.I., 2017. Development of a model to simulate groundwater inundation induced by sea-level rise and high tides in Honolulu, Hawaii. Water Res. 114, 122–134. https://doi.org/10.1016/J.WATRES.2017.02.035

Kreibich, H., Thieken, A.H., 2008. Assessment of damage caused by high groundwater inundation. Water Resour. Res. 44, 9409. https://doi.org/10.1029/2007WR006621

Macdonald, D., Bloomfield, J., Hughes, A., MacDonald, A., Adams, B., McKenzie, A., 2008. Improving the understanding of the risk from groundwater flooding in the UK, in: Flood Risk Management: Research and Practice. pp. 1071–1080. https://doi.org/10.1201/9780203883020.ch125

Markert, K.N., Markert, A.M., Mayer, T., Nauman, C., Haag, A., Poortinga, A., Bhandari, B., Thwal, N.S., Kunlamai, T., Chishtie, F., Kwant, M., Phongsapan, K., Clinton, N., Towashiraporn, P., Saah, D., 2020. Comparing Sentinel-1 Surface Water Mapping Algorithms and Radiometric Terrain Correction Processing in Southeast Asia Utilizing Google Earth Engine. Remote Sens. 2020, Vol. 12, Page 2469 12, 2469. https://doi.org/10.3390/RS12152469

McGaughey, R.J., 2009. FUSION/LDV: Software for LIDAR data analysis and visualization. US Dep. Agric. For. Serv. Pacific Northwest Res. Stn. Seattle, WA, USA 123.

McGuire, V.L., 2017. Water-Level and Recoverable Water in Storage Changes, High Plains Aquifer, Predevelopment to 2015 and 2013-15. U.S. Geol. Surv. Sci. Investig. Rep. 2017–5040 14. https://doi.org/10.3133/SIR20175040

Morris, S.E., Cobby, D., Zaidman, M., Fisher, K., 2018. Modelling and mapping groundwater flooding at the ground surface in Chalk catchments. J. Flood Risk Manag. 11, S251–S268. https://doi.org/10.1111/JFR3.12201

National Climatic Data Center, N.O. and A.A., 2020. No Title [WWW Document]. Online Clim. Data. URL https://www.ncdc.noaa.gov/cdo-web/datasets (accessed 9.22.20).

National Transportation Research, 2022. Key facts about Nebraska’s surface transportation system. WASHINGTON.

Naughton, O., Johnston, P.M., McCormack, T., Gill, L.W., 2017. Groundwater flood risk mapping and management: examples from a lowland karst catchment in Ireland. J. Flood Risk Manag. 10, 53–64. https://doi.org/10.1111/JFR3.12145

Ogilvie, A., Belaud, G., Delenne, C., Bailly, J.-S., Bader, J.-C., Oleksiak, A., Ferry, L., Martin, D., 2015. Decadal monitoring of the Niger Inner Delta flood dynamics using MODIS optical data. J. Hydrol. 523, 368–383. https://doi.org/10.1016/j.jhydrol.2015.01.036

Perica, S., Martin, D., Pavlovic, S., Roy, I., St. Laurent, M., Trypaluk, C., Unruh, D., Yekta, M., Bonnin, G., 2013. NOAA Atlas 14 Volume 8 Version 2, Precipitation-Frequency Atlas of the United States, Midwestern States. NOAA, National Weather Service, Silver Spring, MD.

Peterson, S.M., Flynn, A.T., Traylor, J.P., 2016. Water Availability and Use Science Program Groundwater-Flow Model of the Northern High Plains Aquifer in Colorado, Kansas, Nebraska, South Dakota, and Wyoming Scientific Investigations Report 2016-5153 Time series of simulated and estimated base flow Grou, Scientific Investigations Report. https://doi.org/10.3133/SIR20165153

Peterson, S.M., Traylor, J.P., Guira, M., 2020. Groundwater Availability of the Northern High Plains Aquifer in Colorado, Kansas, Nebraska, South Dakota, and Wyoming, U.S. Geological Survey. https://doi.org/10.3133/pp1864

Pierre-Louis, K. 2021. How rising groundwater caused by climage change could devestate coastal communities. MIT Tecnology Review. https://www.technologyreview.com/2021/12/13/1041309/climate-change-rising-groundwater-flooding/

Pinault, J.L., Amraoui, N., Golaz, C., 2005. Groundwater-induced flooding in macropore-dominated hydrological system in the context of climate changes. Water Resour. Res. 41, 1–16. https://doi.org/10.1029/2004WR003169

Rotzoll, K., Fletcher, C.H., 2012. Assessment of groundwater inundation as a consequence of sea-level rise. Nat. Clim. Chang. 2012 35 3, 477–481. https://doi.org/10.1038/nclimate1725

Scanlon, B.R., Faunt, C.C., Longuevergne, L., Reedy, R.C., Alley, W.M., McGuire, V.L., McMahon, P.B., 2012. Groundwater depletion and sustainability of irrigation in the US High Plains and Central Valley. Proc. Natl. Acad. Sci. U. S. A. 109, 9320–9325. https://doi.org/10.1073/pnas.1200311109

Schumann, G., Matgen, P., Cutler, M.E.J., Black, A., Hoffmann, L., Pfister, L., 2008. Comparison of remotely sensed water stages from LiDAR, topographic contours and SRTM. ISPRS J. Photogramm. Remote Sens. 63, 283–296. https://doi.org/10.1016/j.isprsjprs.2007.09.004

Schumann, G.J.P., Moller, D.K., 2015. Microwave remote sensing of flood inundation. Phys.

Chem. Earth, Parts A/B/C 83–84, 84–95. https://doi.org/10.1016/J.PCE.2015.05.002

Shrestha, N., Mittelstet, A.R., Gilmore, T.E., Zlotnik, V., Neale, C.M., 2021a. Effects of drought on groundwater-fed lake areas in the Nebraska Sand Hills. J. Hydrol. Reg. Stud. 36, 100877. https://doi.org/10.1016/J.EJRH.2021.100877

Shrestha, N., Mittelstet, A.R., Young, A.R., Gilmore, T.E., Gosselin, D.C., Qi, Y., Zeyrek, C., 2021b. Groundwater level assessment and prediction in the Nebraska Sand Hills using LIDAR-derived lake water level. J. Hydrol. 600, 126582. https://doi.org/10.1016/j.jhydrol.2021.126582

Smith, H.T.U., 1965. Dune Morphology and Chronology in Central and Western Nebraska. J. Geol. 73, 557–578. https://doi.org/10.1086/627093

Soylu, M.E., Bras, R.L., 2021. Detecting Shallow Groundwater From Spaceborne Soil Moisture Observations. Water Resour. Res. 57, e2020WR029102. https://doi.org/10.1029/2020WR029102

Strassberg, G., Scanlon, B.R., Chambers, D., 2009. Evaluation of groundwater storage monitoring with the GRACE satellite: Case study of the High Plains aquifer, central United States. Water Resour. Res. 45. https://doi.org/10.1029/2008WR006892

Sweeney, M.R., Loope, D.B., 2001. Holocene dune-sourced alluvial fans in the Nebraska Sand Hills. Geomorphology 38, 31–46. https://doi.org/10.1016/S0169-555X(00)00067-2

Szilagyi, J., Harvey, E., Ayers, J.F., 2003. Regional estimation of base recharge to ground water using water balance and a base-flow index. Groundwater 4, 504-513.

Tiwari, V., Kumar, V., Matin, M.A., Thapa, A., Ellenburg, W.L., Gupta, N., Thapa, S., 2020. Flood inundation mapping- Kerala 2018; Harnessing the power of SAR, automatic threshold detection method and Google Earth Engine. PLoS One 15, e0237324. https://doi.org/10.1371/JOURNAL.PONE.0237324

Töyrä, J., Pietroniro, A., Martz, L.W., Prowse, T.D., 2002. A multi-sensor approach to wetland flood monitoring. Hydrol. Process. 16, 1569–1581. https://doi.org/10.1002/HYP.1021

U.S. Geological Survey, 2016, National Water Information System data available on the World Wide Web (USGS Water Data for the Nation), accessed [February 23, 2025], at URL [http://waterdata.usgs.gov/nwis/].

USGS, 2008. Simulation of ground-water flow and effects of ground-water iirgation on base flow in the Elkhorn and Loup River Basins, Nebraska. https://pubs.usgs.gov/sir/2008/5143/pdf/sir2008_5143.pdf

Vladimir, M., Zhakyp, A., Auelkhan, Y., Yaakov, A., 2024. Assessment of urbanization-related groundwater flooding process via Visual MODFLOW modeling: A case study for the northern part of Almaty city, Kazakhstan. *Journal of Flood Risk Management* 18(1).

Yihdego, Y., Danis, C., & Paffard, A., 2017. Groundwater Engineering in an Environmentally Sensitive Urban Area: Assessment, Landuse Change/Infrastructure Impacts and Mitigation Measures. *Hydrology*, *4*(3), 37. https://doi.org/10.3390/hydrology4030037

Yu, X., Moraetis, D., Nikolaidis, N.P., Li, B., Duffy, C., Liu, B., 2019. A coupled surface-subsurface hydrologic model to assess groundwater flood risk spatially and temporally. Environ. Model. Softw. 114, 129–139. https://doi.org/10.1016/J.ENVSOFT.2019.01.008